ADVANCED MATERIALS

Supporting Information

for *Adv. Mater.*, DOI 10.1002/adma.202309775

Massively Scalable Self-Assembly of Nano and Microparticle Monolayers via Aerosol Assisted Deposition

*Gabriel Cossio, Raul Barbosa, Brian Korgel and Edward T. Yu**

WILEY-VCH

Supporting Information

Title: Massively Scalable Self-Assembly of Nano and Microparticle Monolayers via Aerosol Assisted Deposition

Authors: G. Cossio, R. Barbosa, B. Korgel, E. T. Yu*

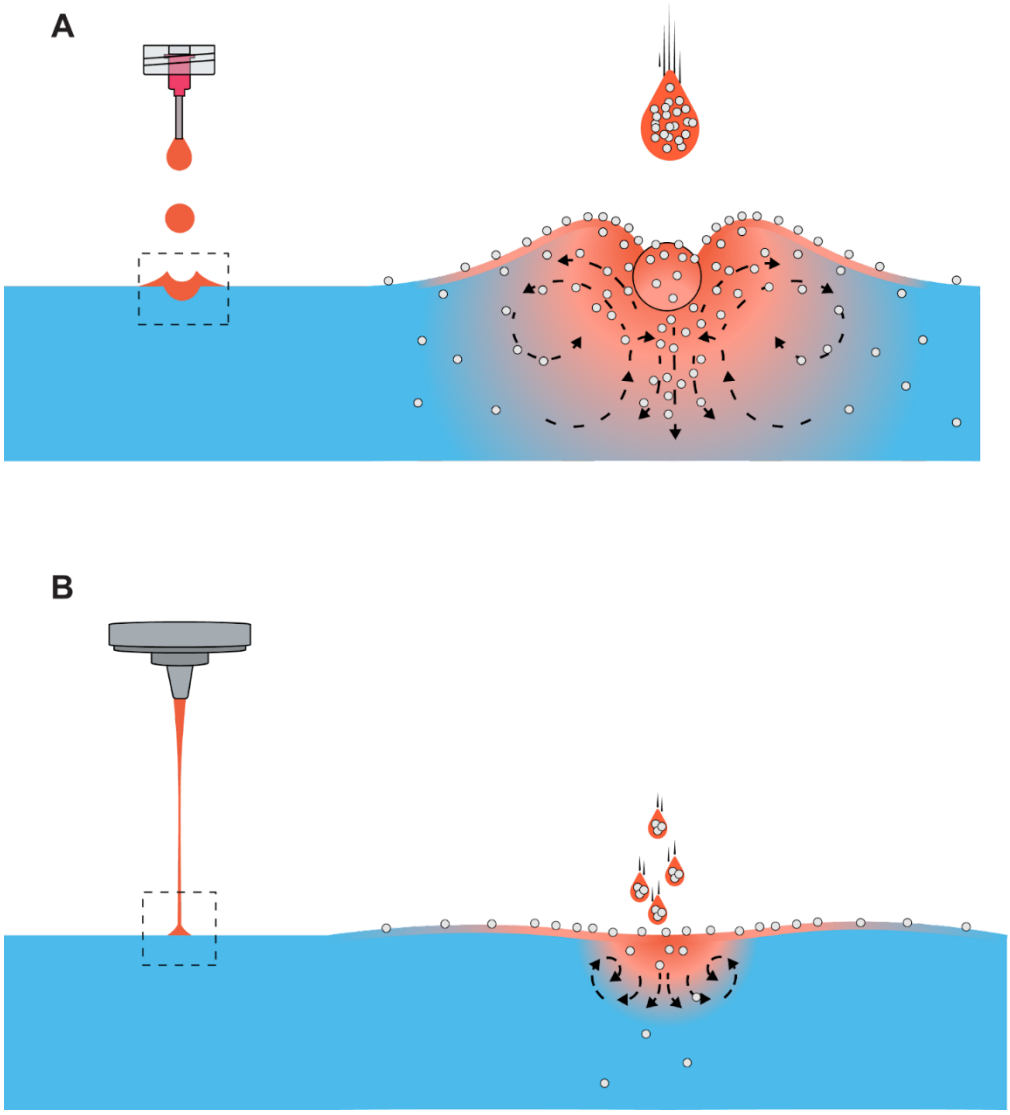

Figure S1. (a) Diagram of liquid dispensing system used in traditional Langmuir-Blodgett microparticle self-assembly. Large millimeter sized droplets of colloidal particles (white circles) in an aqueous alcohol solution (orange droplet) are dropped onto the air-water interface. The large kinetic energy of millimeter sized droplets impinges, greatly deforms, and breaks the surface of the air-water interface dispensing colloidal particles throughout the bulk water volume. Induced vortices (dashed lines) continue to mix microparticles into the bulk water volume decreasing the transfer efficiency of colloidal microparticles to the air-water interface. The surface tension gradient caused by a gradient in the alcohol diffusion (orange) near the point of impact creates the Marangoni force pulling microparticles away from the impact point along the water's surface. (b) Collimated aerosolized beam of micron sized aqueous dispensing droplets (orange droplets) are much smaller in volume and do not have the requisite kinetic energy to break through the water's surface greatly increasing transfer efficiency of colloidal microparticles to the air-water interface. As the water's surface does not break, the diffusion of alcohol into the bulk water volume is reduced and limits the extent of Marangoni induced vortices which can mix colloidal particles into the bulk water volume.

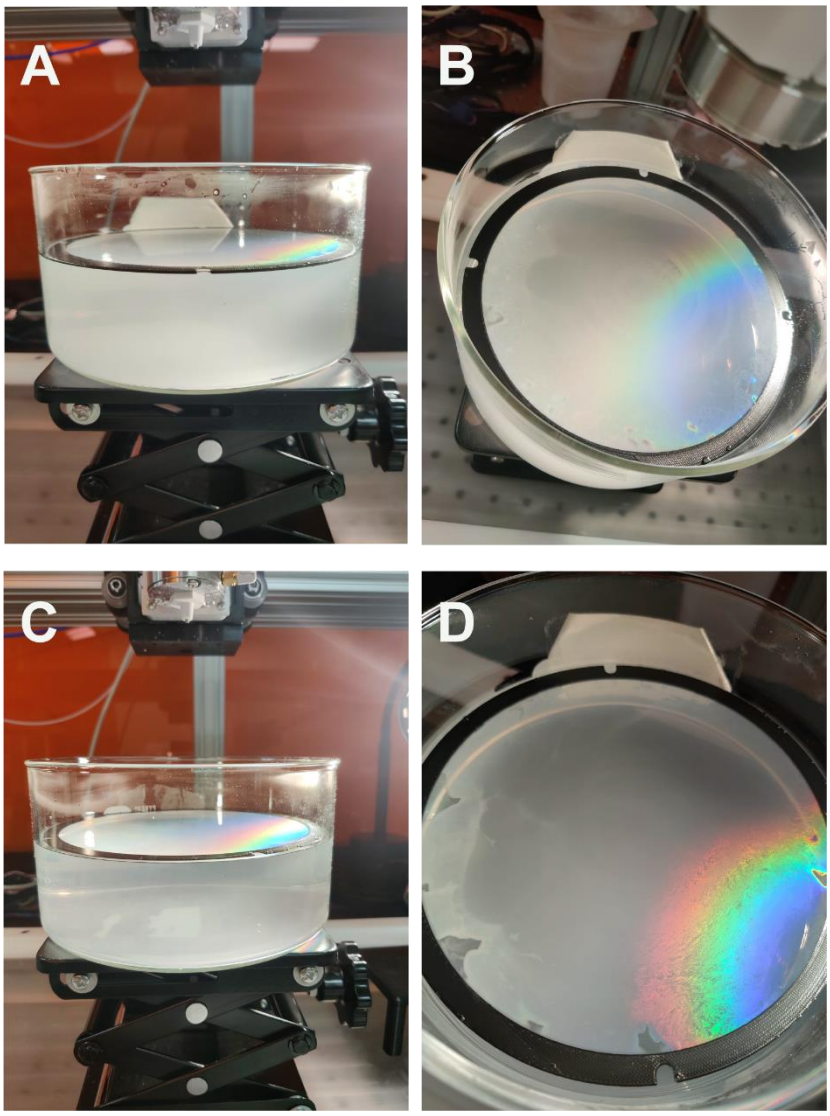

Figure S2. (a) Side view photograph of NP monolayer self-assembled from 1 µm PS NPs via Method 1 at low $|\zeta|$ and low Φ ($|\zeta|$=30 mV, Φ=9x10^{10} NP min^{-1}). (b) Top view of the monolayer shown in (a). (a-b) Photographs show a large concentration of NPs resuspended in the bulk water making the bulk water volume almost opaque and indicating an inefficient transfer of NPs to the air-water interface. The self-assembled demonstrates very low brightness reflection and iridescence consistent with an amorphously arranged NP monolayer. (c) Side view photograph of NP monolayer self-assembled from 1 µm PS NPs via Method 1 at high $|\zeta|$ and high Φ ($|\zeta|$=30 mV, Φ=18x10^{10} NP min^{-1}). (d) Top view of the monolayer shown in (c). (c-d) Photographs show similarly poor transfer efficiency of NPs to air-water interface as (a,b). However, the concentration of resuspended NPs in (c) is lower as demonstrated by the more translucent appearance. Additionally, the monolayer shown in (d) exhibits higher brightness and localized regions of vibrant iridescence.

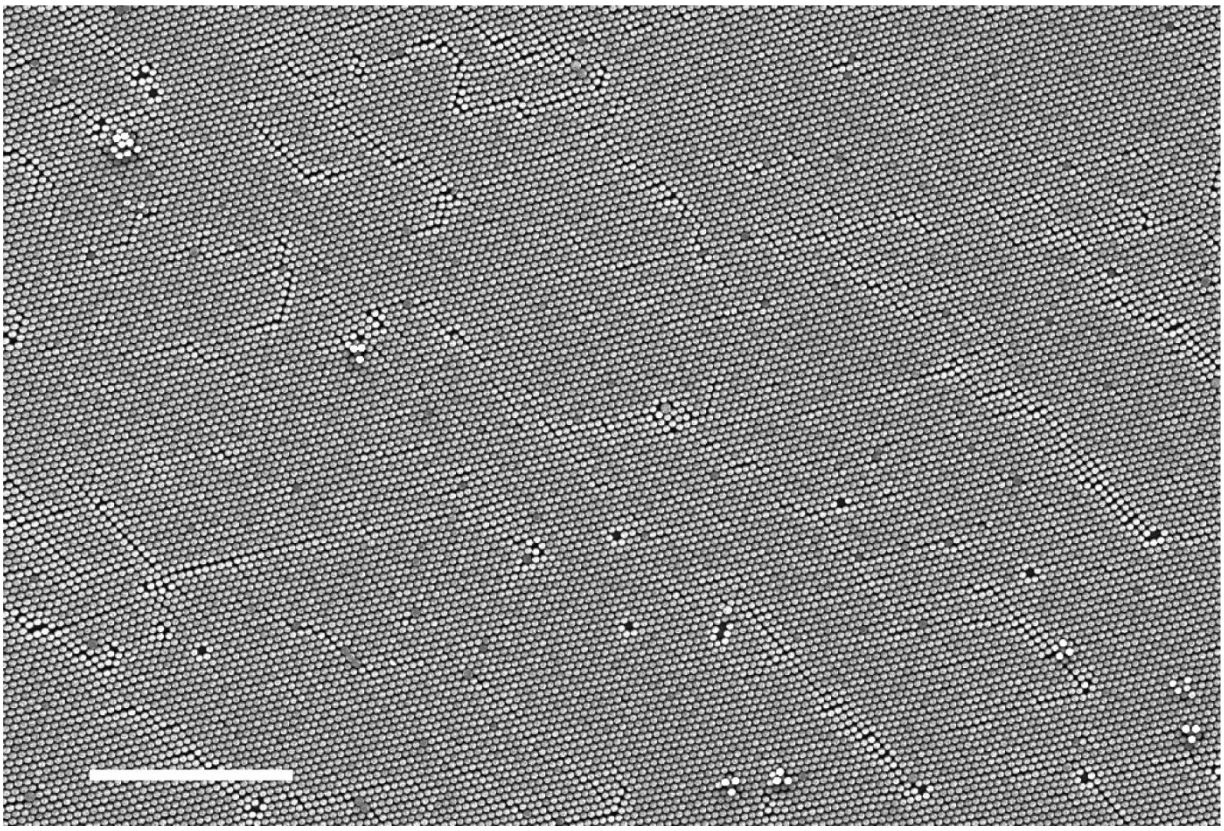

Figure S3. SEM image 2D NP monolayer formed from SDS stabilized 370 nm diameter polystyrene NPs self-assembled via Method 2 at high $|\zeta|$ and Φ ($|\zeta|$=70 mV and Φ =17.5x10^{10} NP min^{-1}). Sample was taken from substrate shown in Figure 4e. Long range crystallinity is shown with minor aggregations and crystal dislocations. Total area is 2341 μm^2. Scale bar is 5 μm.

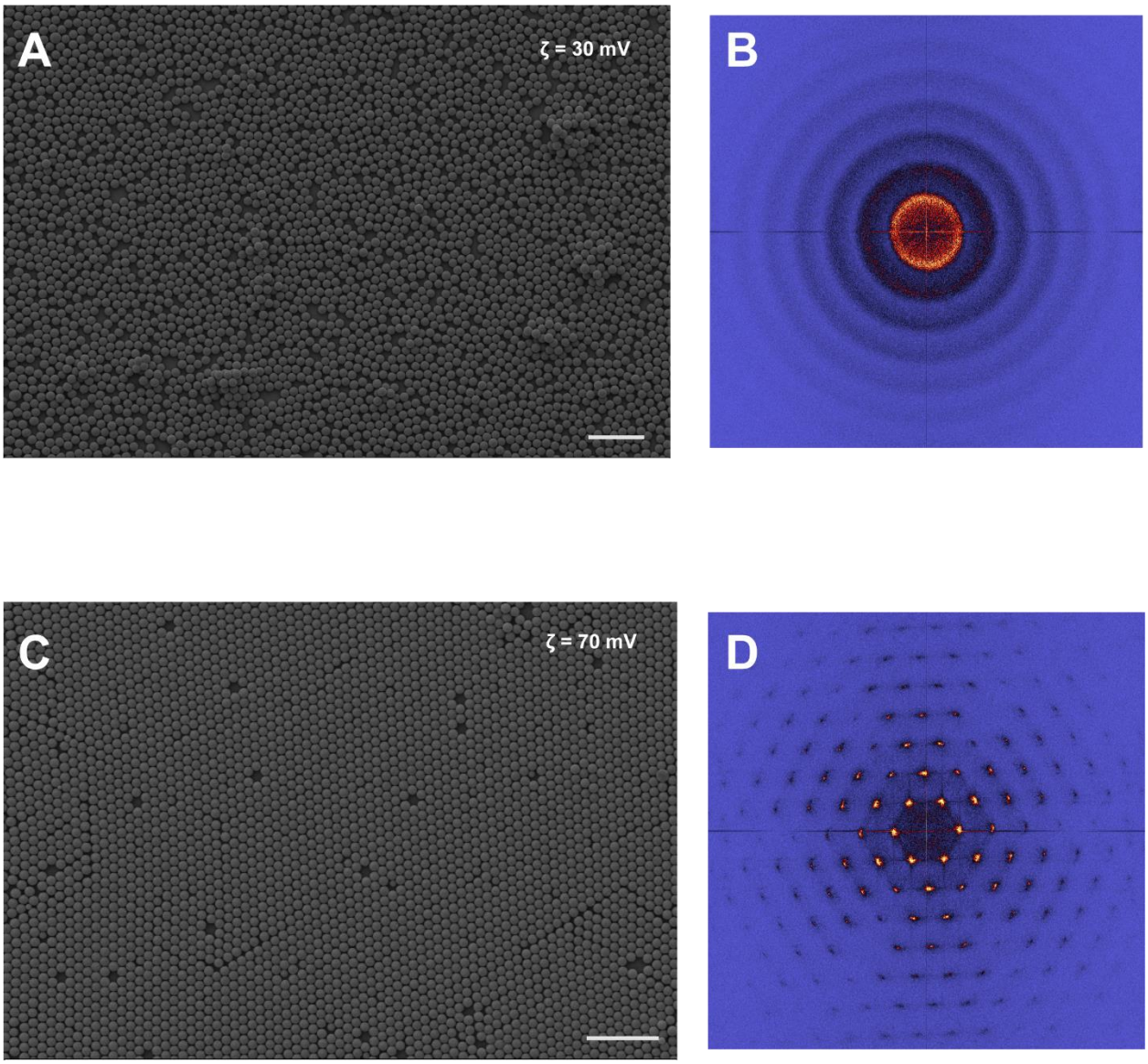

Figure S4. (a) SEM and (b) Fourier transform images of 2D monolayers formed from 700 nm diameter cationic CTAB stabilized polystyrene microparticles self-assembled with low $|\zeta|$ = 30 mV via Method 2. The scale bar in (a) is 4 μm. (c) SEM and (d) Fourier transform images of 2D monolayers formed from 700 nm diameter cationic CTAB stabilized polystyrene microparticles self-assembled with $|\zeta|$ = 70 mV via Method 2. The scale bar in (c) is 5.5 μm.

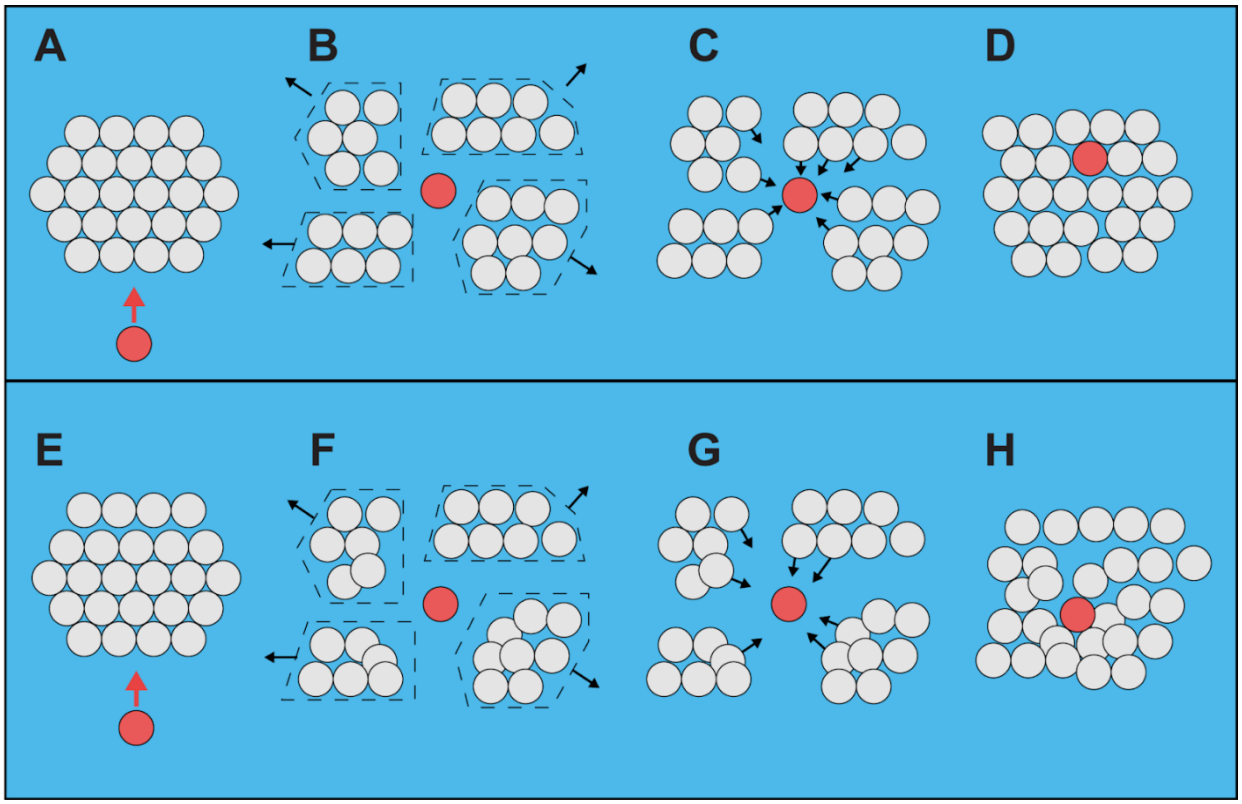

Figure S5. (a-d) Schematic process flow of NP monolayer sself-assembly processes from high $|\zeta|$ colloidal nano or microparticles. (a) A new microparticle (red) obtains kinetic energy from the Marangoni force and is introduced to a newly formed array of microparticles (white). (b) The new microparticle collides with the crystal and transfers energy and momentum to neighboring microparticles introducing disorder and fragmentation of the crystal. (c) The impinging and neighboring particles reach a new equilibrium. As the Marangoni force dissipates the water's surface contracts to bring the particles into a new crystalline arrangement. (d) The high $|\zeta|$ of the microparticles prevents their aggregation and promotes ordered self-assembly of the microparticles in successive colloidal crystal fragmentation and re-growth. (e-h) Schematic process flow of NP monolayer self-assembly processes from low $|\zeta|$ colloidal nano or microparticles. (e) A new microparticle (red) obtains kinetic energy from the Marangoni force and is introduced to a newly formed array of microparticles (white). (f) The new microparticle collides with the crystal though it's low colloidal stability (due to its low $|\zeta|$) causes it to stick to other particles in the collision. Similarly, neighboring microparticles which were in other scattering events can form aggregations with adjacent particles. (g) As the surface of the water contracts new scattering events are created and form additional aggregations. (h) A final larger array is formed with decreased order and amorphous packing and large particle aggregations.

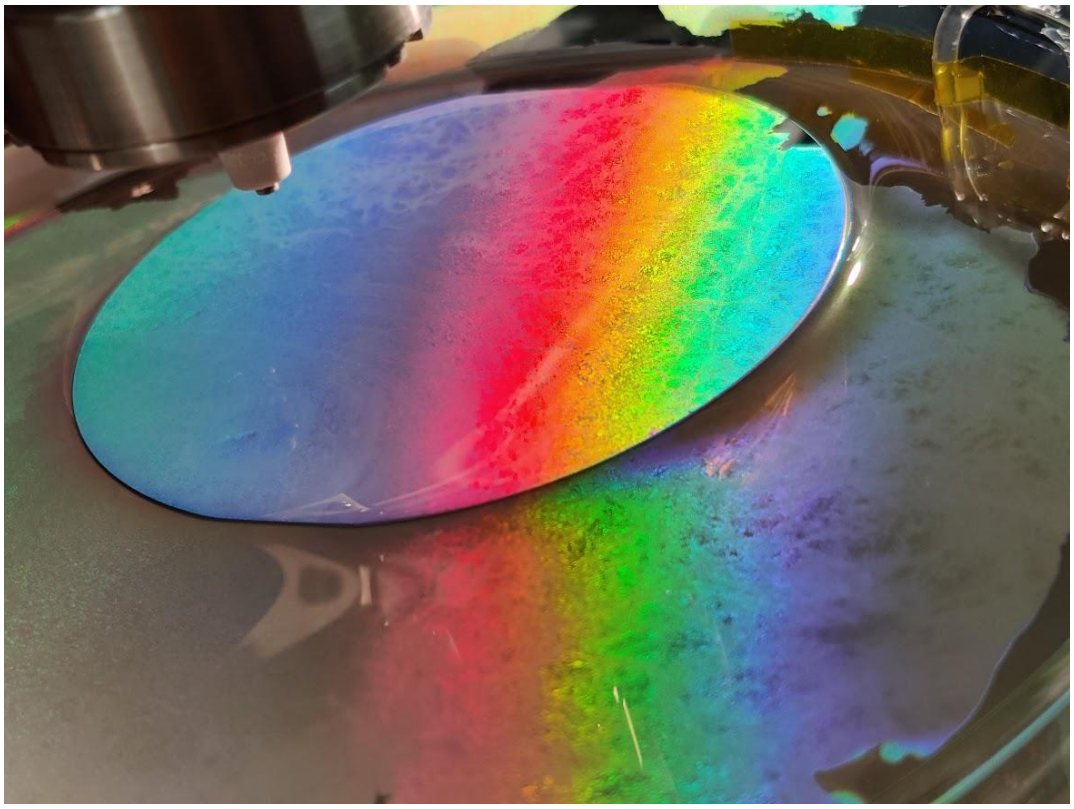

Figure S6. Photograph a 1 µm PS NP monolayer self-assembled via Method 1 being transferred to a 4'' silicon wafer (ζ = -70 mV, $\Phi = 18x10^{10}$ NPs min^{-1}). The self-assembled NP monolayer appears distinctly different from the highly ordered monolayers shown in Figure 4f (main text). Amorphously arranged NP monolayer displays lower intensity brightness, diffuse reflectance, and almost no macroscopically distinguishable crystalline domains.

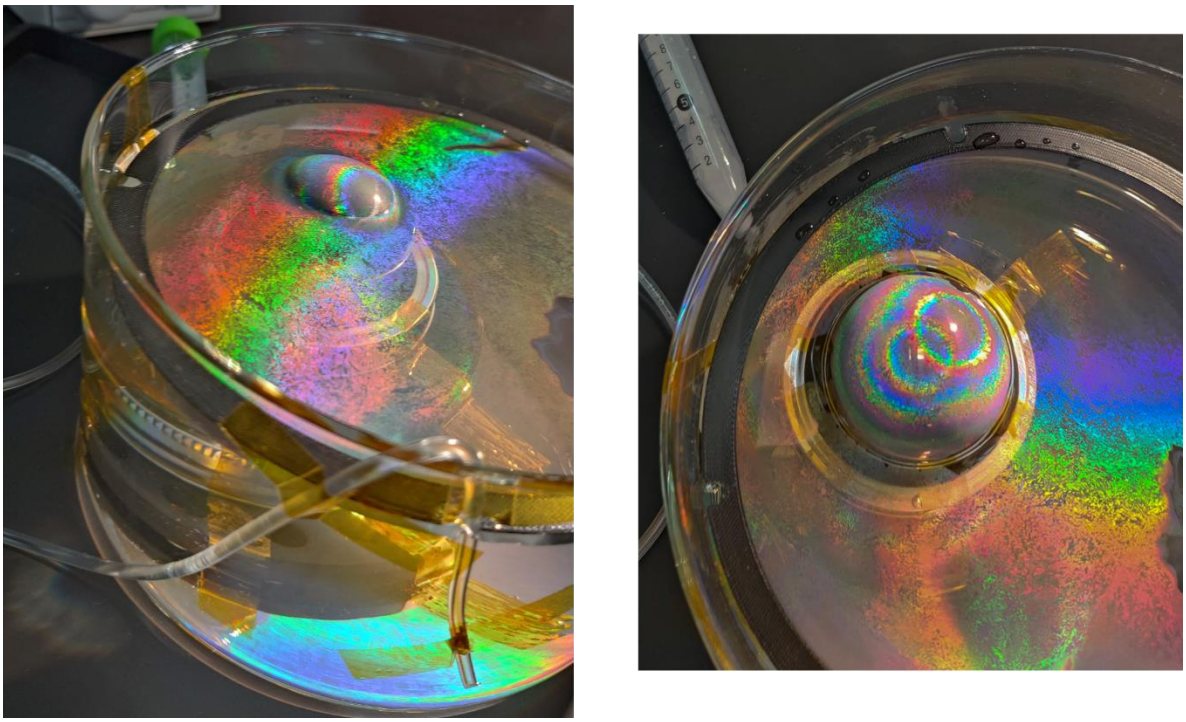

Figure S7. (Left) Side view photograph of the self-assembled 1 μm PS NP monolayer being transferred to the sphere shown in **Figure 4g** of the main text. As the liquid is drained from the reservoir, the monolayer at the air-water interface conforms to and is deposited onto the curved surface of the sphere. (Right) Top view photograph of the self-assembled 1 μm PS NP monolayer being transferred to the sphere shown in **Figure 4g** of the main text. The photograph was taken at a later time in the draining process, as can be seen by the larger area of the NP monolayer which has been transferred to the spherical substrate. The bottom half of the sphere is masked with Kapton tape to prevent the monolayer from transfering to this area to provide better surface contrast.

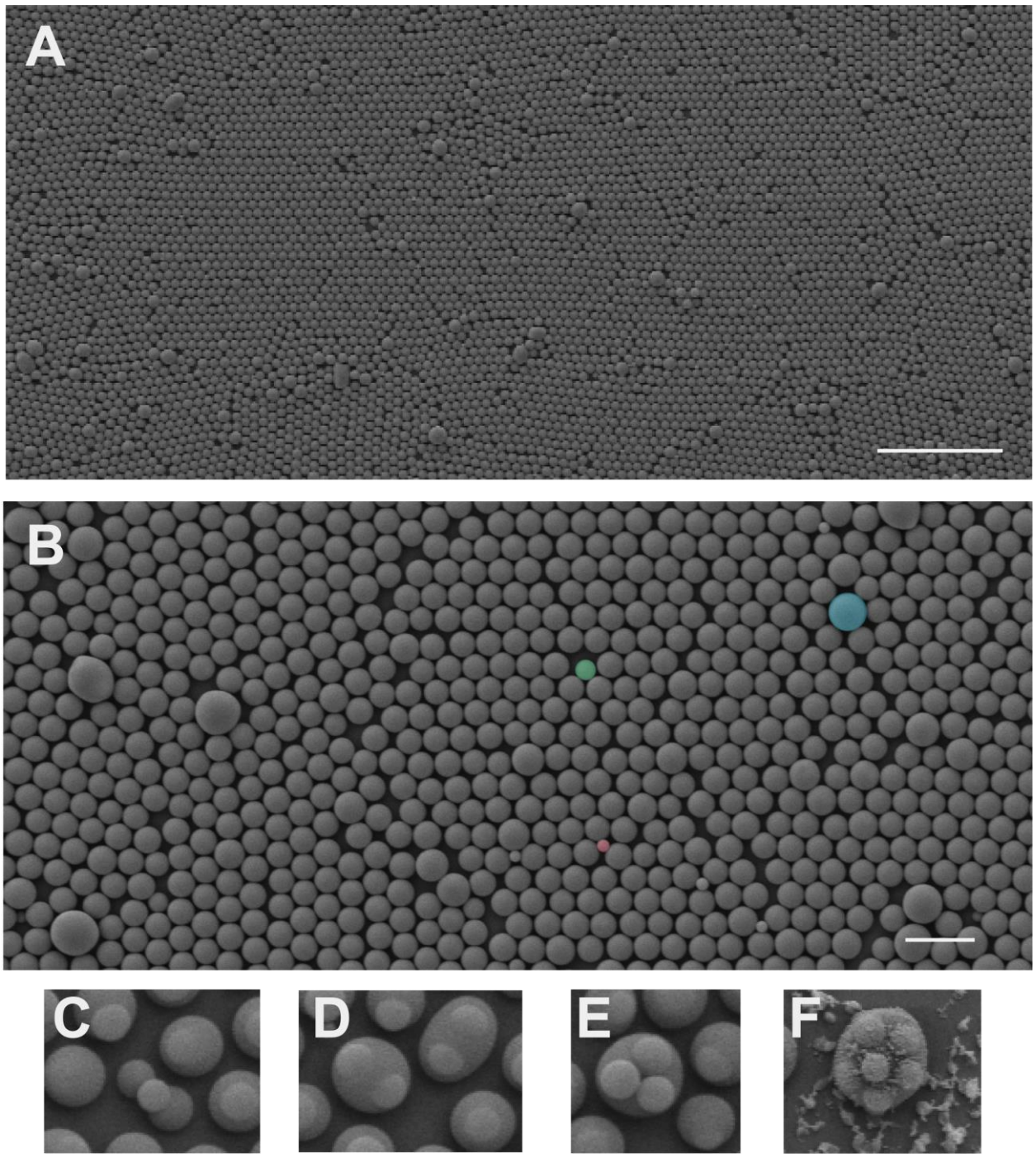

Figure S8. (a) SEM image of self-assembled monolayer of core-shell SiO2@TiO2@PS colloidal particles. Self-assembled monolayer shows long-range order that is disturbed by large multi-cored particles. Scale bar is 10 µm. (b) Close-up image of (a) demonstrating that array defects are primarily formed by large multi-core particles (blue), pure polystyrene particles (green), and un-shelled particles (red). Scale bar is 2 µm. (c-f) SEM images of various non-ideal core-shell particles contributing to a loss of long-range order due to polydispersity in the self-assembled monolayer. Lobed growth (c), doublet (d), triplet (e), and higher order multi-core particles (f). Core diameters are 350 nm in all images.

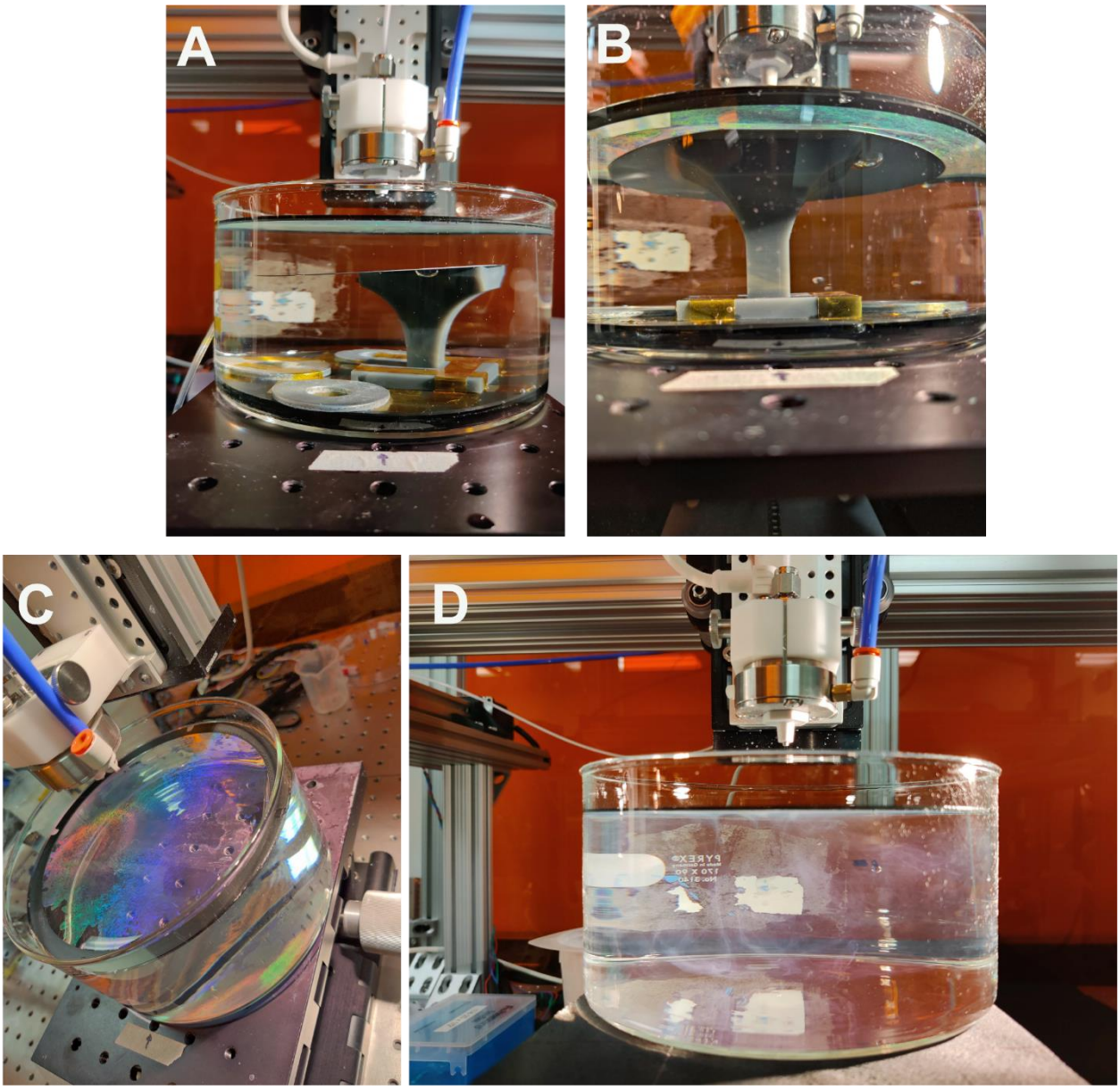

Figure S9. (a-b) Photographs of retaining beaker immediately after the self-assembly of 370 nm diameter PS NPs via Method 2 ($|\zeta|$ = 70 mV, $\Phi = 17.5 \times 10^{10}$). The 370 nm diameter PS NP monolayer can be seen in the reflection at the air-water interface. Virtually no NPs can be seen resuspended in the bulk water volume demonstrating the high transfer efficiency of NPs to the air-water interface. (c) Top view photograph of a 1µm diameter PS NP monolayer self-assembled via Method 2 ($|\zeta|$ = 70 mV, $\Phi = 17.5 \times 10^{10}$). (d) Photograph showing 1µm diameter PS NP resuspended in the bulk water volume when self-assembling an NP monolayer via Method 2. The deposition was continued for three seconds after the monolayer annulus (Figure 1c, Figure 4a-d main text) was fully closed demonstrating that the air-water interface was fully saturated with NPs.